2021

Prediction of Lubricant Viscosity from Nonequilibrium Molecular Dynamics Simulation

Lingnan Lin
National Institute of Standards and Technology, United States of America, lingnan.lin@nist.gov

Mark Kedzeriski

Prediction of Lubricant Viscosity from Nonequilibrium Molecular Dynamics Simulation

Lingnan LIN*, Mark KEDZIERSKI

National Institute of Standards and Technology,
Gaithersburg, Maryland, USA
301-975-6441, lingnan.lin@nist.gov

* Corresponding Author

ABSTRACT

Nonequilibrium molecular dynamics simulation (NEMD) was used to compute the viscosity of a pure polyol ester, pentaerythritol tetrahexanoate (PEC6), for a broad range of strain rate (10^7 s^{-1} to 10^{10} s^{-1}), temperature (258 K to 373 K), and pressure (0.1 MPa to 1 GPa). The Newtonian viscosity was obtained by fitting the viscosities at different strain rates to the Eyring model. The predicted Newtonian viscosities agree well with the experimental data with respect to temperature and pressure. The molecular dynamics simulation is pure prediction because it requires only the chemical structure as the input. Therefore, molecular dynamics can be especially useful in simulating those hypothetical molecules and those experimentally inaccessible conditions, which can reduce the cost and time of experimentation and facilitate the development of high-performance lubricants.

1. INTRODUCTION

Viscosity is one of the most important properties of a lubricant, because it is inherently linked to the lubricant hydrodynamics and has a profound impact on compressor performance and reliability (Xu & Hrnjak, 2017). A decrease in viscosity will cause thinning of the lubricant film and may cause equipment failure if the viscosity is too low, while an excessively large viscosity can lead to increased motor loading and higher power consumption (Michels & Sienel, 2003). These characteristics are key considerations when choosing the viscosity grade of a lubricant. At present, the research on refrigeration lubricants relies heavily upon experimental measurement and correlation. Unfortunately, the data are very limited, especially for extreme conditions where measurements are difficult to perform. On the other hand, the advance of alternative low-GWP refrigerants necessitates the co-development of lubricants. For these reasons, quantitative approaches are needed that can be used to predict lubricant properties, like viscosity, from knowledge of only the chemical structure. Equipped with such techniques, scientists could sift through a tremendous number of potential lubricant structures in a much more rational manner, thereby more readily discovering compounds with desired properties for a given application.

In recent years, molecular dynamics (MD) simulation has been used to compliment experimentation and to study thermodynamic and transport properties. For example, nonequilibrium molecular dynamics (NEMD) simulations have been used to compute lubricant viscosities. In NEMD, an external field (perturbation) is applied to the equations of motion and the response of the system at non-equilibrium steady state is sampled to obtain the viscosity. Most of the studied lubricants are hydrocarbon based, such as n-hexadecane (Ewen et al., 2016), 1-Decene trimer (Liu et al., 2015), poly-α-olefin (PAO) (Kioupis & Maginn, 1999), and 9-octylheptadecane (McCabe et al., 2001); whereas refrigeration lubricants like polyol ester (POE) are rarely found in the literature. This is unfortunate given that POE is one of the most widely used refrigeration lubricants (Bruno et al., 2019). A POE molecule features one or more ester groups as well as long and branched molecular architecture, which is more complex than the structure of hydrocarbons and makes the NEMD simulation more challenging.

In this study, nonequilibrium molecular dynamics (NEMD) simulation was used to to compute the viscosity of a typical, pure polyol ester, pentaerythritol tetrahexanoate (PEC6, $C_{29}H_{52}O_8$, see Figure 1) for temperatures from 258 K to 373 K and pressures from 0.1 MPa to 1 GPa. The prediction was compared with the experimental data in the literature.

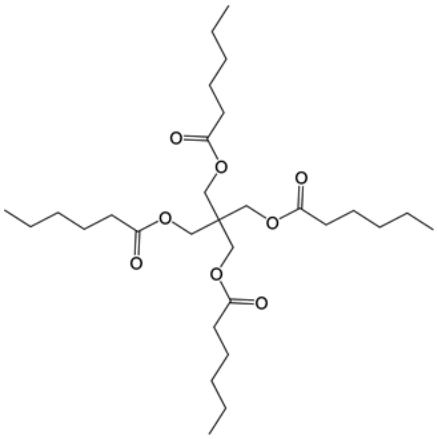

Figure 1. Chemical structure of pentaerythritol tetrahexanoate (PEC6)

2. METHOD

Fundamentally, molecular dynamics (MD) is the simulation of the time evolution of the atomistic positions (i.e., trajectory) of a molecular system. This is done by integrating the Newton's equations of motion for every atom in the system:

$$m_i \frac{d^2}{dt^2}\mathbf{r}_i = \mathbf{F}_i \tag{1}$$

where m_i, $\mathbf{r}_i$, and $\mathbf{F}_i$ are mass, position and force of the i-th atom, respectively. The force term is calculated from the potential energy $U_{\mathrm{pe}}(\mathbf{r}_1, \mathbf{r}_2, \dots, \mathbf{r}_N)$:

$$\mathbf{F}_i = -\frac{\partial}{\partial \mathbf{r}_i} U_{\mathrm{pe}}(\mathbf{r}_1, \mathbf{r}_2, \dots, \mathbf{r}_N) \tag{2}$$

A force field is used here to determine the potential energy U_{pe}. With the trajectory generated by the MD simulation, properties like density and viscosity can be derived.

2.1 Force field

The force field is basically a set of functions and parameters that are used to model the interactions in the molecular system. The total potential energy of a molecular system can be expressed by the sum of the molecular energy components:

$$U_{\mathrm{pe}} = U_{\mathrm{elec}} + U_{\mathrm{vdw}} + U_{\mathrm{bond}} + U_{\mathrm{angle}} + U_{\mathrm{torsion}} + U_{\mathrm{improper}} \tag{3}$$

where U_{elec} and U_{vdw} represent non-bonded interactions of electrostatic interaction and van der Waals interaction, respectively; U_{bond}, U_{angle}, U_{torsion}, U_{improper} represent bonded interactions corresponding to contributions of bond stretching, angle bending, internal rotation around the dihedral angle (torsion), and out-of-plane bending (improper torsion), respectively.

The all-atom force field LOPLS (Pluhackova et al., 2015; Siu et al., 2012) was used because it was optimized for esters and long hydrocarbons. The energy potential functions used by LOPLS are:

$$
\begin{cases}
U_{\text{elec}} = \dfrac{1}{4\pi\varepsilon_0}\dfrac{q_i q_j}{r_{ij}} \\
U_{\text{vdw}} = 4\varepsilon_{ij}\left[\left(\dfrac{\sigma_{ij}}{r_{ij}}\right)^{12} - \left(\dfrac{\sigma_{ij}}{r_{ij}}\right)^{6}\right] \\
U_{\text{bond}} = K_r(r - r_0)^2 \\
U_{\text{angle}} = K_\theta(\theta - \theta_0)^2 \\
U_{\text{torsion}} = \dfrac{V_1}{2}[1 + \cos(\phi)] + \dfrac{V_2}{2}[1 - \cos(2\phi)] + \dfrac{V_3}{2}[1 + \cos(3\phi)] \\
U_{\text{improper}} = K_\chi(\chi - \chi_0)^2
\end{cases}
\tag{4}
$$

where r, θ, ϕ, and χ are bond length, bond angle, proper dihedral angle, and improper dihedral angle, respectively; K_r, r_0, K_θ, θ_0, V_1, V_2, V_3, K_χ, χ_0, ε_{ij}, σ_{ij} are force field parameters; q is partial charge. The LOPLS parameters can be found in Pluhackova et al. (2015) and Siu et al. (2012).

2.2 Viscosity calculation

In NEMD simulations, a planar Couette flow was set up by continuously deforming the simulation box with a constant strain rate using the SLLOD equations of motion (Evans & Morriss, 2008). The volume and temperature were maintained constant with the Nose/Hover thermostat (Hoover, 1985). The shear viscosity (i.e., shear-dependent viscosity) was calculated from the stress tensor:

$$\eta(\dot{\gamma}) = -\frac{\langle P_{xy}\rangle}{\dot{\gamma}} \tag{5}$$

where $\eta(\dot{\gamma})$ is the shear viscosity, P_{xy} is the xy component of the stress tensor, $\dot{\gamma}$ is the shear rate: $\dot{\gamma} = \partial u_x/\partial y$ (i.e., the gradient of the streaming velocity at flow direction, u_x, along the y axis).

The stress tensor **P** is given by the virial theorem:

$$\mathbf{P}V = \sum_i \frac{\mathbf{p}_i\mathbf{p}_i}{m_i} + \sum_i \mathbf{r}_i\mathbf{F}_i \tag{6}$$

where $\mathbf{p}_i$ is the momentum, m_i is the mass, $\mathbf{r}_i$ is the position vector, and $\mathbf{F}_i$ is the force acting on the ith atom.

In typical NEMD simulations, the shear rate generally should be higher than 10^8 s^{-1} to overcome the thermal noise (Cui et al., 1998; Lu et al., 2019). At such high shear rates, the lubricant may transition to the non-Newtonian regime, where the viscosity becomes a function of shear rate, while in experiments the viscosity is measured in the Newtonian regime, where the viscosity is independent of shear rate. To obtain the Newtonian viscosity that corresponds to experiment, NEMD simulations were performed at varying shear rates to calculate the shear viscosities and to extrapolate to the Newtonian (zero-shear) viscosity. The shear viscosities were fit to the Eyring model (Ewell & Eyring, 1937; Eyring, 1936):

$$\dot{\gamma} = \frac{\sigma_{\text{E}}}{\eta_{\text{N}}}\sinh\left(\frac{\langle P_{xy}\rangle}{\sigma_{\text{E}}}\right) \tag{7}$$

where σ_{E} and η_{N} are the Eyring stress and the Newtonian viscosity, respectively. Combining Equations (5) and (7), an explicit form of η can be written as:

$$\eta = \frac{\sigma_{\text{E}}}{\dot{\gamma}}\ln\left(\frac{\eta_{\text{N}}}{\sigma_{\text{E}}}\dot{\gamma} + \sqrt{\left(\frac{\eta_{\text{N}}}{\sigma_{\text{E}}}\dot{\gamma}\right)^2 + 1}\right) \tag{8}$$

The Newtonian viscosity, η_N, can be solved for from the Eyring fit (equation (8)) once the η data have been determined by NEMD simulations.

2.3 Simulation details

MD simulations were performed using the LAMMPS package (Plimpton, 1995) for temperature from 258 K to 373 K and pressure from 0.1 MPa to 1 GPa. LAMMPS data files that contain the information of molecular topology, force field parameters, etc., were prepared using Moltemplate (Jewett, 2019). Force field parameters were manually checked to ensure that the values are in accordance with those in the literature of origin. The simulations were conducted in cubic boxes with periodic boundary conditions in all directions. The standard velocity-Verlet algorithm (Verlet, 1967) was used to integrate the equations of motion with a timestep of 0.5 fs. A total of 125 molecules (125 × 89 atoms) were used in all simulations. The Nosé−Hoover thermostat (Hoover, 1985) and the extended Lagrangian approach (Shinoda et al., 2004) were applied to control the temperature and the pressure, respectively, unless otherwise stated. The thermostat and barostat time constants were 50 fs and 500 fs, respectively. The Lennard-Jones interactions were truncated at 1.2 nm and long-range tail corrections were applied for the energy and pressure calculation. The electrostatic interactions were calculated using the particle−particle particle−mesh (PPPM) method (Hockney & Eastwood, 1988) with a real space cutoff of 1.2 nm and a precision of 10^{-4} beyond the cutoff distance.

The equilibration of the system was started with a conjugate gradient energy minimization (Polak & Ribiere, 1969) for the initial configuration. Then a "simulated annealing process" (Kirkpatrick et al., 1983) was performed to avoid the trapping of the molecular structure in conformations that represent local minima. In the annealing process, the system was first heated to 490 K at p = 0.1 MPa and then slowly cooled (with a rate of 15 K/ns) to each target temperature at constant volume (NVT). When a target temperature was reached, another 10 ns NVT run was carried out to fully relax the system. Then the system was simulated with a barostat (NPT) at the chosen p to find the appropriate density for 25 ns in which the averaged density was calculated over the last 5 ns. Longer equilibration times were used for elevated pressures. In the course of the equilibration, properties like temperature and pressure, as well as kinetic and potential energy, were monitored to ensure they reached steady state. The final configuration from the NPT equilibration run was resized to match the averaged density, followed by another NVT run for 20 ns. The resulting configuration served as the initial configuration for later NEMD simulations for the viscosity calculation.

In NEMD simulation, the system was sheared at fixed density and shear rate $\dot{\gamma}$ using the SLLOD equations of motion (Evans & Morriss, 2008). The stress tensor and other relevant state variables were monitored to determine if and when the steady state was reached. These variables were averaged and output every 10^6 time steps (i.e., 50 ps). The steady states were reached in a time of approximately $\dot{\gamma}^{-1}$ for all studied state points. After reaching steady state, the simulation was run for another 25 ns (40 ns for p > 500 MPa) and the shear stress was averaged over the last 20 ns (30 ns for p > 500 MPa) to obtain $\langle P_{xy} \rangle$ and compute the shear viscosity $\eta(\dot{\gamma})$ using Eq. (5). Block averaging and autocorrelation analysis (Grossfield et al., 2019) were performed for each production trajectory to assess the sampling quality and to calculate the uncertainty. Longer production length gave equivalent results on the scale of the symbol size in our plots. The procedure was repeated for various $\dot{\gamma}$ to obtain a spectrum of $\eta(\dot{\gamma})$ that covers Newtonian and non-Newtonian regimes. The range of $\dot{\gamma}$ varies with the temperature due to the shift of $\dot{\gamma}_c$. The simulated $\dot{\gamma}$ extends from 10^7 s^{-1} to 10^{10} s^{-1}, and no heating or other nonequilibrium effects were observed in this range. The obtained $\eta(\dot{\gamma})$ as a function of $\dot{\gamma}$ was then fit to the Eyring model to calculate η_N. The regression was performed with weights $\omega_i = 1/u_i^2$ (u_i is the expanded uncertainty of $\eta(\dot{\gamma}_i)$) using the Levenberg-Marquardt algorithm (Press et al., 1988). The weights were used to cancel out different degrees of noise at different $\dot{\gamma}$ and to propagate the uncertainty of $\eta(\dot{\gamma})$ to η_N.

The code and data files for the simulations are publicly available at: https://github.com/LL8848/viscosity_nemd.

3. RESULTS

Figure 2 shows the shear viscosities computed from NEMD simulations as a function of shear rate ($\dot{\gamma}$) for different temperatures (258 K to 373 K, 0.1 MPa). The error bars to either side of the symbols represent the degree to which the viscosity fluctuates in the course of NEMD simulations. The fluctuation of viscosity is mainly caused by the thermal motion of molecules, or "thermal noise". The atomistic positions continuously fluctuate as a result of thermal motion, leading to the fluctuation of the system's momenta and total potential energy, which both contribute to the

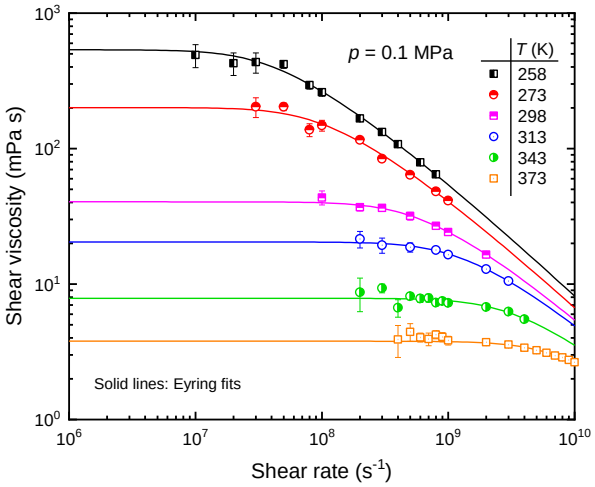

Figure 2. Shear dependence of viscosity for different temperatures.

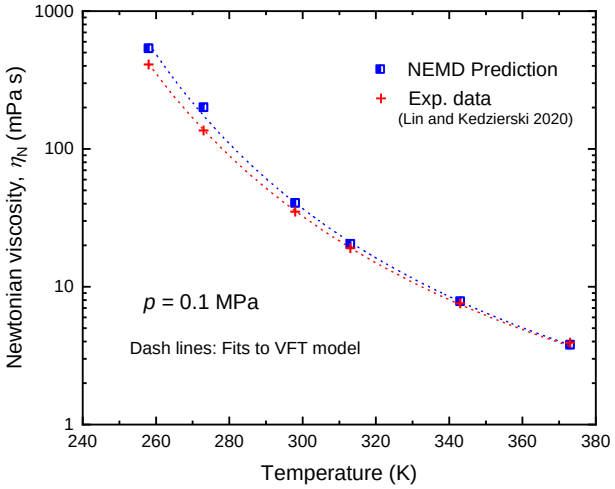

Figure 3. Temperature dependence of Newtonian viscosity.

stress tensor **P**, and consequently cause the viscosity to fluctuate ($\eta = P_{xy}/\dot{\gamma}$). As shown in Fig. 2, the fluctuation of viscosity intensifies as the shear rate decreases. This is because the shear stress decreases with decreasing shear rate while the thermal noise remains unchanged, resulting in a decrease of signal-to-noise ratio. At low shear rates, where the fluctuations are significant, the response of the lubricant molecules to the shear perturbation is relatively weak compared to the thermal motion. Note that the thermal motion is temperature dependent, thus the errors are relatively larger at higher temperatures for the same shear rate.

As shown in Fig. 2, the viscosity of PEC6 plateaus at low shear rate (i.e., Newtonian regime) and decreases with increasing shear rate at high shear rate (i.e., shear thinning). The critical shear rate $\dot{\gamma}_c$ at which the lubricant transitions from Newtonian regime to shear-thinning is higher at higher temperature. The increased $\dot{\gamma}_c$ with increasing temperature can be explained by the mechanism of shear induced molecular alignment (Cui et al., 1998; Daivis & Evans, 1994). Under low shear rates, the shear imposed on molecules can be balanced out by the molecular relaxation. When the shear rate exceeds a critical value, which is approximately the inverse of the longest relaxation time, molecules cannot respond fast enough to the shear deformation as caused by the flow field, and consequently tend to align with the flow field to relieve the stress. The molecular alignment leads to a reduced viscosity of the lubricant, i.e., shear shinning. At higher temperature, the molecules move and rotate more quickly, resulting in a shorter relaxation time and therefore a higher $\dot{\gamma}_c$.

The solid lines in Fig. 2 are the best-fit regressions of the NEMD-computed shear viscosities $\eta(\dot{\gamma})$ to the Eyring model (Eq. 8). It can be seen that the shear viscosities are well fit by the Eyring model for the range of simulated shear rates. The extrapolation of a fit to low shear rates equals to the Newtonian viscosity. Figure 3 shows the Newtonian viscosity η_N as a function of temperature obtained from Eyring fits. The dash lines in Fig. 3 are the best-fit regressions of η_N to the VFT model:

$$\log \eta_N = A + \frac{B}{T - T_0} \tag{9}$$

The predicted η_N are compared with the experimental data (Lin & Kedzierski, 2020). The deviation between the predicted η_N and the measurement is between 3 % and 47 % for 258 K to 373 K. The relatively large deviation at low temperature is partly due to the increased uncertainties of η_{NEMD} and η_N with decreasing temperature.

Figure 4 shows the computed shear viscosities for pressures up to 1 GPa with the temperature fixed at 373 K. The critical shear rate $\dot{\gamma}_c$ (i.e., the onset of shear-thinning) decreases with increasing pressure. With the pressure increased from 0.1 MPa to 1 GPa, $\dot{\gamma}_c$ increases from 4.5×10^9 s^{-1} to 3.4×10^6 s^{-1} as estimated by the Eyring fits. Figure 5 shows the Newtonian viscosity η_N as a function of pressure obtained from Eyring fits. The prediction is compared with the experimental data from Ref. (Bair, 2019b). The η_N for lower pressures (≤ 100 MPa) match the experimental data very well (within ± 10 %), whereas they start to diverge at 300 MPa. However, the less-than-exponential rising trend of

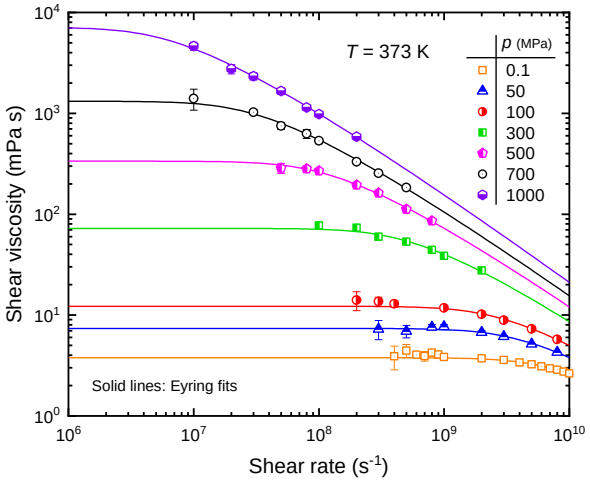

Figure 5. Shear dependence of viscosity for different pressures.

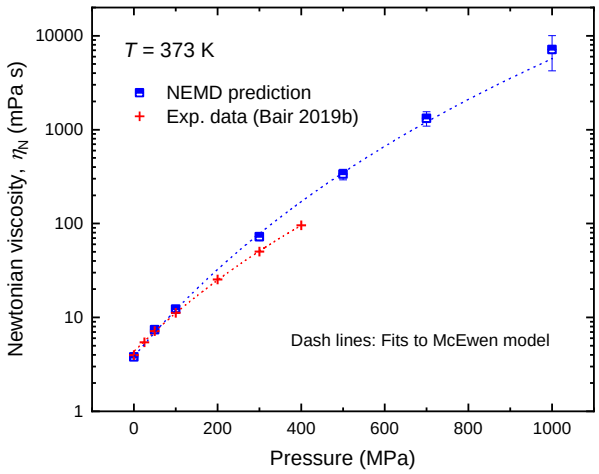

Figure 4. Pressure dependence of Newtonian viscosity.

η_N with respect to pressure, as exhibited by the experimental data, is reproduced by the prediction. The data as well as the predictions are therefore fit to the McEwen model which is widely used to model less-than-exponential pressure–viscosity response (Bair, 2019a):

$$\eta_N = \eta_0 \left(1 + \frac{\alpha_0}{q} p\right)^q \tag{10}$$

where $\eta_0 = 4.3385$, $\alpha_0 = 0.0102$ and $q = 5.8433$ for the experimental data and $\eta_0 = 3.8225$, $\alpha_0 = 0.0124$ and $q = 7.4961$ for the predictions. Note that the McEwen fit slightly diverges from the predicted η_N at 1 GPa, indicating that there may be a transition of pressure–viscosity response from less-than-exponential to exponential at between 800 MPa and 1000 MPa.

4. DISCUSSION AND CONCLUSIONS

The results demonstrated that the NEMD simulation with LOPLS force field adequately describes the rheology behavior of POE lubricant. The viscosity prediction is in satisfactory agreement with measurements for a broad range of temperature and pressure. The only input is the molecular topology (or chemical structure) of the lubricant. It is a *pure prediction* considering the facts: (i) PEC6 or similar POE molecules (i.e., pentaerythritol tetraesters) were not used for the parametrization of the LOPLS force field; (ii) the parameters of the LOPLS force field were optimized for density and heat of vaporization, without explicit consideration of transport properties. The results also confirmed the transferability of the LOPLS force field, meaning that it can be applied to predict other POE lubricants and perhaps other classes of lubricants. This will be especially useful for simulating hypothetical molecules that haven't been synthesized, which is of great significance in optimizing the performance of existing lubricants and guiding the design and synthesis of new lubricants.

The deviation between the predicted viscosity and the measurement indicates that the prediction accuracy could be improved by further refining the force field parameters. Despite the deviation of absolute values, the NEMD simulation accurately captured the relative change in viscosity. In practice, trends in properties are as valuable as the quantitative accuracy in property predictions. This viscosity computation method can be used to study many other lubricant problems, such as the pressure–viscosity relation, the effect of molecular architecture on viscosity, etc.

In addition to viscosity, MD can also be used to predict other lubricant properties, such as solubility and thermal conductivity. Physical insights at the atomistic and molecular level can also be obtained from the simulations. As such, we believe that MD is a powerful tool for the lubricant research and development.

NOMENCLATURE

English symbols		Greek symbols	
F	force	$\dot{\gamma}$	shear rate
m	mass	η	viscosity
P	stress tensor	η_{N}	Newtonian viscosity
p	pressure	θ	bond angle
p	momentum	ρ	density
q	partial charge	σ_{E}	Eyring stress
r	position	ϕ	proper dihedral angle
r	bond length	χ	improper dihedral angle
T	temperature		
U	energy, uncertainty		
u	error		

REFERENCES

Bair, S. (2019a). Correlations for the Temperature and Pressure and Composition Dependence of Low-Shear Viscosity. In *High Pressure Rheology for Quantitative Elastohydrodynamics* (pp. 135–182). Elsevier. https://doi.org/10.1016/B978-0-444-64156-4.00006-4

Bair, S. (2019b). The Pressure and Temperature Dependence of the Low-Shear Viscosity. In *High Pressure Rheology for Quantitative Elastohydrodynamics* (Vol. 39, Issue 10, pp. 97–133). Elsevier. https://doi.org/10.1016/B978-0-444-64156-4.00005-2

Bruno, T. J., Fortin, T. J., Huber, M. L., Lemmon, E. W., Mclinden, M. O., Outcalt, S. L., Perkins, R. A., Urness, K. N., Widegren, J. A., Bruno, T. J., Fortin, T. J., Mansfield, E., & Mclinden, M. O. (2019). Thermophysical Properties of Polyol Ester Lubricants. In *NIST Technical Note 8263*.

Cui, S. T., Cummings, P. T., Cochran, H. D., Moore, J. D., & Gupta, S. A. (1998). Nonequilibrium molecular dynamics simulation of the rheology of linear and branched alkanes. *International Journal of Thermophysics*, *19*(2 SPEC.ISS.), 449–459. https://doi.org/10.1023/A:1022565427881

Daivis, P. J., & Evans, D. J. (1994). Comparison of constant pressure and constant volume nonequilibrium simulations of sheared model decane. *The Journal of Chemical Physics*, *100*(1), 541–547. https://doi.org/10.1063/1.466970

Evans, D. J., & Morriss, G. (2008). Statistical mechanics of nonequilibrium liquids, second edition. In *Statistical Mechanics of Nonequilibrium Liquids, Second Edition*. https://doi.org/10.1017/CBO9780511535307

Ewell, R. H., & Eyring, H. (1937). Theory of the Viscosity of Liquids as a Function of Temperature and Pressure. *The Journal of Chemical Physics*, *5*(9), 726–736. https://doi.org/10.1063/1.1750108

Ewen, J. P., Gattinoni, C., Thakkar, F. M., Morgan, N., Spikes, H. A., & Dini, D. (2016). A comparison of classical force-fields for molecular dynamics simulations of lubricants. *Materials*, *9*(8), 1–17. https://doi.org/10.3390/ma9080651

Eyring, H. (1936). Viscosity, Plasticity, and Diffusion as Examples of Absolute Reaction Rates. *The Journal of Chemical Physics*, *4*(4), 283–291. https://doi.org/10.1063/1.1749836

Grossfield, A., Patrone, P. N., Roe, D. R., Schultz, A. J., Siderius, D., & Zuckerman, D. M. (2019). Best Practices for Quantification of Uncertainty and Sampling Quality in Molecular Simulations [Article v1.0]. *Living Journal of Computational Molecular Science*, *1*(1), 1–24. https://doi.org/10.33011/livecoms.1.1.5067

Hockney, R. W., & Eastwood, J. W. (1988). *Computer Simulation Using Particles*. IOP Publishing Ltd. https://doi.org/10.1887/0852743920

Hoover, W. G. (1985). Canonical dynamics: Equilibrium phase-space distributions. *Physical Review A*, *31*(3), 1695–1697. https://doi.org/10.1103/PhysRevA.31.1695

Jewett, A. (2019). *Moltemplate. https://www.moltemplate.org/*. https://www.moltemplate.org/

Kioupis, L. I., & Maginn, E. J. (1999). Molecular Simulation of Poly-α-olefin Synthetic Lubricants: Impact of Molecular Architecture on Performance Properties. *The Journal of Physical Chemistry B*, *103*(49), 10781–10790. https://doi.org/10.1021/jp992399n

Kirkpatrick, S., Gelatt, C. D., & Vecchi, M. P. (1983). Optimization by simulated annealing. *Science*, *220*(4598), 671–680. https://doi.org/10.1126/science.220.4598.671

Lin, L., & Kedzierski, M. (2020). Density and viscosity of a polyol ester lubricant: Measurement and molecular dynamics simulation. *International Journal of Refrigeration*, *118*, 188–201. https://doi.org/10.1016/j.ijrefrig.2020.07.004

Liu, P., Yu, H., Ren, N., Lockwood, F. E., & Wang, Q. J. (2015). Pressure-Viscosity Coefficient of Hydrocarbon Base Oil through Molecular Dynamics Simulations. *Tribology Letters*, *60*(3), 1–9. https://doi.org/10.1007/s11249-015-0610-6

Lu, J., Wang, Q. J., Ren, N., & Lockwood, F. E. (2019). Correlation between pressure-viscosity coefficient and traction coefficient of the base stocks in traction lubricants: A molecular dynamic approach. *Tribology International*, *134*(February), 328–334. https://doi.org/10.1016/j.triboint.2019.02.013

McCabe, C., Cui, S., & Cummings, P. T. (2001). Characterizing the viscosity–temperature dependence of lubricants by molecular simulation. *Fluid Phase Equilibria*, *183–184*, 363–370. https://doi.org/10.1016/S0378-3812(01)00448-4

Michels, H. H., & Sienel, T. H. (2003). Refrigeration Lubricants- Properties and Applications. In *Fuels and Lubricant Handbook: Technology, Properties, Performance, and Testing* (pp. 413–430). ASTM International.

Plimpton, S. (1995). Fast Parallel Algorithms for Short-Range Molecular Dynamics. *Journal of Computational Physics*, *117*(1), 1–19. https://doi.org/10.1006/jcph.1995.1039

Pluhackova, K., Morhenn, H., Lautner, L., Lohstroh, W., Nemkovski, K. S., Unruh, T., & Böckmann, R. A. (2015). Extension of the LOPLS-AA Force Field for Alcohols, Esters, and Monoolein Bilayers and its Validation by Neutron Scattering Experiments. *The Journal of Physical Chemistry B*, *119*(49), 15287–15299. https://doi.org/10.1021/acs.jpcb.5b08569

Polak, E., & Ribiere, G. (1969). Note sur la convergence de méthodes de directions conjuguées. *Revue Française d'informatique et de Recherche Opérationnelle. Série Rouge*, *3*(16), 35–43. https://doi.org/10.1051/m2an/196903R100351

Press, W. H., Teukolsky, S. A., Vetterling, W. T., & Flannery, B. P. (1988). *Numerical Recipes in C, Ch. 15.5, Nonlinear Models*. Cambridge University Press.

Shinoda, W., Shiga, M., & Mikami, M. (2004). Rapid estimation of elastic constants by molecular dynamics simulation under constant stress. *Physical Review B*, *69*(13), 134103. https://doi.org/10.1103/PhysRevB.69.134103

Siu, S. W. I., Pluhackova, K., & Böckmann, R. A. (2012). Optimization of the OPLS-AA Force Field for Long Hydrocarbons. *Journal of Chemical Theory and Computation*, *8*(4), 1459–1470. https://doi.org/10.1021/ct200908r

Verlet, L. (1967). Computer "Experiments" on Classical Fluids. I. Thermodynamical Properties of Lennard-Jones Molecules. *Physical Review*, *159*(1), 98–103. https://doi.org/10.1103/PhysRev.159.98

Xu, J., & Hrnjak, P. (2017). Quantification of flow and retention of oil in compressor discharge pipe. *International Journal of Refrigeration*, *80*, 252–263. https://doi.org/10.1016/j.ijrefrig.2017.05.004

ACKNOWLEDGEMENT

This work was funded by the National Institute of Standards and Technology (NIST), United States. Thanks go to the following NIST personnel for their constructive criticism of the draft manuscript: A. Pertzborn, M. Huber, and G. Linteris. The computations were performed on the NIST High Performance Computing (HPC) Clusters.